

# ADAPTIVE SHOOT-THROUGH DUTY RATIO CONTROL METHODOLOGY OF STAND-ALONE QUASI Z-SOURCE INVERTER

Pritam Kumar Gayen<sup>1</sup>– Pijush Kanti Dhara<sup>2</sup> – Sudip Das<sup>3\*</sup> – Alok Shrivastav<sup>3</sup>

<sup>1</sup>Department of Electrical Engineering, Kalyani Government Engineering College, Kalyani, West Bengal, India

<sup>2</sup>Department of Energy Science and Engineering, Indian Institute of Technology Bombay, Mumbai, India

<sup>3</sup>Department of Electrical Engineering, JIS College of Engineering, Kalyani, West Bengal, India

## ARTICLE INFO

### Article history:

Received: 11.05.2023.

Received in revised form: 16.07.2023.

Accepted: 17.11.2023.

### Keywords:

Quasi Z-source Inverter

Shoot-through Duty Ratio Control

Stand-alone Operation

Voltage Stress

Total Harmonic Distortion

DOI: <https://doi.org/10.30765/er.2251>

## Abstract:

*This paper presents an adaptive shoot-through duty ratio control methodology for a stand-alone three-phase quasi-Z-source inverter (qZSI). In practice, variable active and reactive load powers must be met by a qZSI-based stand-alone system. In this context, existing shoot-through control schemes for qZSI adjust the capacitor voltage or DC-link voltage at a fixed reference value. This causes extra voltage stresses on switches, high distortions, and an operating range reduction of the power inverter under variable load demands. On the contrary, the proposed shoot-through control scheme adjusts the shoot-through duty ratio adaptively based on load voltage feedback to improve performances. In this logic, the controllable shoot-through duty ratio facilitates various improved features in comparison to conventional schemes under load power variations. These features include reduced voltage stress across the switches, reduced distortions, and an extended operating range. The suggested proportional-integral (PI)-based scheme has a single control loop with a single measured quantity, i.e., sensing of load voltage only. The proposed concept has been verified via both simulation and experimental studies.*

## 1 Introduction

In earlier days, the combination of a DC-DC converter and a pulse width modulated (PWM) voltage source inverter was extensively used in various applications for converting dc voltage to the required ac voltage [1, 2]. Various disadvantages of this two-stage DC-AC conversion system have been removed by the introduction of a single converter topology, namely the Z-source inverter (ZSI) [3]. In this context, the design, operation, and control methodologies of ZSI are presented in the published papers [4-8]. The main drawbacks of ZSI are the unsteady input current drawn from the DC source, the uncommon ground between the source and load, and the higher voltage stresses on the capacitor. Therefore, the quasi Z-source inverter (qZSI) topology is introduced as an improved version of ZSI to overcome its limitations [9]. The schematic diagram of qZSI in stand-alone loading conditions is shown in Figure 1. The qZSI uses an impedance network comprising two capacitors ( $C_1, C_2$ ), two inductors ( $L_1, L_2$ ), and a diode ( $D$ ) at its input side to facilitate voltage boosting action.

The modelling, and design of qZSI are presented in various published literatures [10-12]. From the application point of view, various shoot-through control schemes for ZSI and qZSI have been developed, and these are thoroughly reviewed in [13]. Here, the input-side shoot-through duty ratio control loop can boost up the input voltage level of the inverter bridge to an expected fixed value. In the schemes, different working variables are used as boosted up inverter input voltage, capacitor voltage, and peak value of DC-link voltage

\* Corresponding author

E-mail address: [sudipdas1380@gmail.com](mailto:sudipdas1380@gmail.com)

in different control loops for generating the required shoot-through duty ratio [14-16]. The output-side closed loop control scheme is functionally a voltage regulation loop [17]. It adjusts the modulation index (MI) to get the standard output voltage for the load. In its stand-alone mode of operation, the input and output side control schemes for qZSI are simultaneously used in various literatures to meet load requirements [18, 19]. Here, the coordinated operation between two control loops is an important issue. The various pulse width modulation (PWM) methods are used for ZSI/qZSI, namely the simple boost control (SBC) [3], maximum boost control (MBC) [20], and maximum constant boost control (MCBC) [21] methods. Various space vector control techniques of qZSI are compared in [22]. The existing control schemes keep the DC control signals equal to or greater than the peak of the modulating signal. The MBC-based closed loop action provides the least switch voltage stress and highest gain among other conventional methods [8]. But the main drawback of an MBC-based closed loop scheme is the generation of low-frequency ripple in the inductor current. Thus, qZSI requires a larger inductor to suppress the ripple current under the MBC-controlled mode of operation. Therefore, the MCBC method is the optimum choice because it provides moderate voltage gain along with low-frequency ripple-free operation.

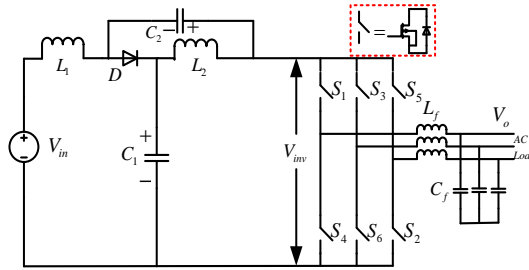


Figure 1. qZSI topology

The traditional control schemes target constant DC bus voltage ( $\hat{V}_{inv}$ ) under variable loads. Thus, the schemes increase voltage stress, losses, and total harmonic distortion (THD). This paper concentrates on the simple and single-loop control structure, that facilitates adaptive shoot-through duty ratio control to achieve desired output voltage regulation while supplying isolated variable loads. This results in various improved features, such as the reduction of switch voltage stress and THD, low losses, and an extended operating range. Both simulation and experimental studies have been carried out to justify the proposed concept and the above-mentioned performance objectives. The fundamentals of qZSI are presented in section 2. Section 3 describes the proposed control scheme and associated meritorious points. Section 4 is devoted to presenting the results of simulation studies and experimental work to validate the suggested concept. It presents the conclusions in section 5.

## 2 Basics of qZSI

The fundamental equations are outlined in this section. The qZSI has an additional state of operation along with the active and zero states. This incorporated state is a shoot-through state. The active and zero states together are called the non-shoot-through state. The peak value of the input voltage ( $\hat{V}_{inv}$ ) of inverter bridge is given by,

$$\hat{V}_{inv} = \frac{1}{1-2D_{sh}} V_{dc} = BV_{in} \tag{1}$$

$$B = \frac{1}{1-2D_{sh}} \tag{2}$$

Where ‘ $D_{sh}$ ’ is shoot-through duty ratio, ‘ $B$ ’ is boosting factor. Finally, peak value of output ac voltage ( $\hat{V}_o$ ) is,

$$\hat{V}_0 = MBV_{dc}/2 \quad (3)$$

Here, ‘ $M$ ’ is modulation index.

From (3), the overall voltage gain ( $G$ ) is defined as,

$$G = BM = \frac{1}{1 - 2D_{sh}} M \quad (4)$$

### 2.1 Parameter calculations

The ripples in inductor currents are expressed as,

$$\begin{cases} \Delta I_{L1} = \frac{D_{sh}(1 - D_{sh})}{(1 - 2D_{sh})} \cdot \frac{V_{in}}{2L_1F_s} \\ \Delta I_{L2} = \frac{D_{sh}(1 - D_{sh})}{(1 - 2D_{sh})} \cdot \frac{V_{in}}{2L_2F_s} \end{cases} \quad (5)$$

The inductor values are computed as,

$$\begin{cases} L_1 = \frac{D_{sh}(1 - D_{sh})}{(1 - 2D_{sh})} \cdot \frac{V_{in}}{2\Delta I_{L1}F_s} = \frac{D_{sh}(1 - D_{sh})BV_{in}}{2\Delta I_{L1}F_s} \\ L_2 = \frac{D_{sh}(1 - D_{sh})}{(1 - 2D_{sh})} \cdot \frac{V_{in}}{2\Delta I_{L2}F_s} = \frac{D_{sh}(1 - D_{sh})BV_{in}}{2\Delta I_{L1}F_s} \end{cases} \quad (6)$$

The input current supplied by the DC voltage source is mathematically expressed as,

$$I_{in} = \frac{3}{8} \frac{M^2}{(1 - 2D_{sh})^2} \frac{V_{in}}{R} \quad (7)$$

The ‘ $R$ ’ in (7) indicates load resistance in Ohm. The averaged inductor currents are given by,

$$\begin{cases} I_{L1} = \frac{3}{8} \frac{M^2}{(1 - 2D_{sh})^2} \frac{V_{in}}{R} \\ I_{L2} = \frac{3}{8} \frac{M^2}{(1 - 2D_{sh})^2} \frac{V_{in}}{R} \end{cases} \quad (8)$$

The averaged current in DC-link point is,

$$I_{dc} = \frac{3}{8} \frac{M^2}{(1 - D_{sh})(1 - 2D_{sh})} \frac{V_{in}}{R} \quad (9)$$

The capacitor voltage ripples are derived as,

$$\begin{cases} \Delta V_{C1} = \frac{3}{8} \frac{D_{sh} M^2}{(1-2D_{sh})^2} \frac{V_{in}}{2RC_1 F_s} \\ \Delta V_{C2} = \frac{3}{8} \frac{D_{sh} M^2}{(1-2D_{sh})^2} \frac{V_{in}}{2RC_2 F_s} \end{cases} \quad (10)$$

The capacitances are estimated as,

$$\begin{cases} C_1 = \frac{3}{8} \frac{D_{sh} M^2}{(1-2D_{sh})^2} \frac{V_{in}}{2R\Delta V_{C1} F_s} \\ C_2 = \frac{3}{8} \frac{D_{sh} M^2}{(1-2D_{sh})^2} \frac{V_{in}}{2R\Delta V_{C2} F_s} \end{cases} \quad (11)$$

### 2.2 Various stresses on different elements

The voltage and current stresses of different elements of impedance networks are derived and presented in Table 1.

Table 1. Various stresses

Parameter	Voltage Stress	Parameter	Current Stress
C <sub>1</sub>	(1-D <sub>sh</sub> ) BV <sub>in</sub>	L <sub>1</sub>	{1/(1-D <sub>sh</sub> )} BI <sub>dc</sub>
C <sub>2</sub>	D <sub>sh</sub> BV <sub>in</sub>	L <sub>2</sub>	{1/(1-D <sub>sh</sub> )} BI <sub>dc</sub>
D	BVin	D	{1/(1-D <sub>sh</sub> ) <sup>2</sup> } BI <sub>dc</sub>

### 2.3 Losses and efficiency

The expressions of losses occurred in different elements of qZSI are presented in Table 2.

Table 2. Current and Loss expressions

Element	Current	Loss
L:	$\begin{cases} I_{L1(RMS)} = \frac{(1-D_{sh})}{(1-2D_{sh})} I_{DC} \\ I_{L2(RMS)} = \frac{(1-D_{sh})}{(1-2D_{sh})} I_{DC} \end{cases}$	$P_L = I_{L1(RMS)}^2 r_{L1} + I_{L2(RMS)}^2 r_{L2}$
C:	$\begin{cases} I_{C1(RMS)} = \frac{\sqrt{D_{sh} \cdot (1-D_{sh})}}{(1-2D_{sh})} I_{DC} \\ I_{C2(RMS)} = \frac{\sqrt{D_{sh} \cdot (1-D_{sh})}}{(1-2D_{sh})} I_{DC} \end{cases}$	$P_C = I_{C1(RMS)}^2 r_{C1} + I_{C2(RMS)}^2 r_{C2}$
D:	$I_{D(AVG)} = \frac{(1-D_{sh})}{(1-2D_{sh})} I_{DC};$ $I_{D(RMS)} = \frac{\sqrt{(1-D_{sh})}}{(1-2D_{sh})} I_{DC}$	$\begin{cases} P_{rr} = Q_{rr} F_s \hat{V}_{inv} \\ P_{fd} = I_{D(AVG)} \cdot V_F \\ P_{oh} = I_{D1(RMS)}^2 r_D \\ P_D = P_{rr} + P_{fd} + P_{oh} \end{cases}$
S <sub>1-6</sub> :	$I_{S_{inv}(RMS)} = \sqrt{\frac{D_{sh}}{9} \cdot I_{sh}^2 + \frac{16(1-D_{sh})P_o^2}{9\pi^2 M^2 B^2 V_{inv}^2 \cdot \cos^2 \phi}}$ $I_{Sh} = I_{L1} + I_{L2}$	$\begin{cases} P_{SW(INV)} = 6 \cdot \frac{(T_{ON} + T_{OFF})}{2} \cdot F_s \cdot \hat{V}_{in} \cdot \frac{I_{sh}}{3} \\ P_{COND(INV)} = 6 \cdot I_{S_{inv}(RMS)}^2 \cdot r_{S_{inv}} \end{cases}$ $P_{sw} = P_{SW(INV)} + P_{COND(INV)}$
Efficiency: $\eta = \frac{V_{in} I_{L1} - (P_L + P_C + P_D + P_{sw})}{V_{in} I_{L1}}$		

### 3 Proposed control scheme

The mutual relationships between ‘ $D_{sh}$ ’, and ‘ $M$ ’, for various PWM methods are presented in Table 3.

Table 3. Relationship between  $D_{sh}$  and  $M$

Existing Method	Relation
Simple Boost Control (SBC)	$D_{sh}(\max) = 1 - M$
Maximum Boost Control (MBC)	$D_{sh} = 1 - (3\sqrt{3}M / 2\pi)$
Maximum Constant Boost Control (MCBC)	$D_{sh} = 1 - (\sqrt{3}M / 2)$

The adaptive shoot-through control logic used in the study is presented in Figure 2

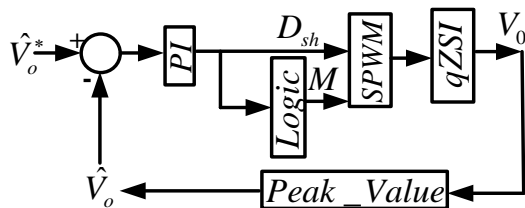


Figure 2. Proposed control logic diagram

The main aim of the proposed control scheme for qZSI is to supply variable active and reactive powers for dynamic loads in a stand-alone mode of operation with its various improved operational features. The PWM methodology is considered a sine-triangle PWM along with DC signals. The modulating sine signal is compared with a triangular high-frequency carrier signal to produce an active (i.e.,  $\text{Sine} > \text{Triangle}$ ) and zero-state (i.e.,  $\text{Sine} < \text{Triangle}$ ). On the other hand, DC signals are compared with the same carrier signal for producing a shoot-through duty ratio ( $D_{sh}$ ). Due to load variation, the output load voltage will be changed. Consequently, the changed load cannot be tackled by the qZSI without voltage regulating action. In this respect, the qZSI can be controlled as per the proposed closed loop action presented in Figure 2 to maintain a standard output load voltage irrespective of load variation.

This adaptive scheme has a single closed loop structure with an output voltage sensing requirement only. Figure 2 reveals that only the required shoot-through duty ratio is controlled by the PI controller. Here, the ‘ $M$ ’ is simultaneously generated from the adaptive shoot-through duty ratio through any PWM logic mentioned in Table 3. On the contrary, both MI and shoot-through duty ratios are separately controlled in conventional control approaches. In the suggested scheme, the control philosophy is to vary the shoot-through duty ratio to obtain the required overall voltage gain for supplying variable load powers.

#### 4 Results and discussion

The specifications of passive components and controller gains used in simulation and experimental studies are given in Table 4 and Table 5 respectively.

Table 4. Values of passive parameters

Existing Method	Relation
$L_1, L_2$	0.5 mH
$C_1, C_2$	300 $\mu\text{F}$
Filter inductance ( $L_f$ )	3 mH
Filter capacitance ( $C_f$ )	50 $\mu\text{F}$

Table 5. Values of controller gains

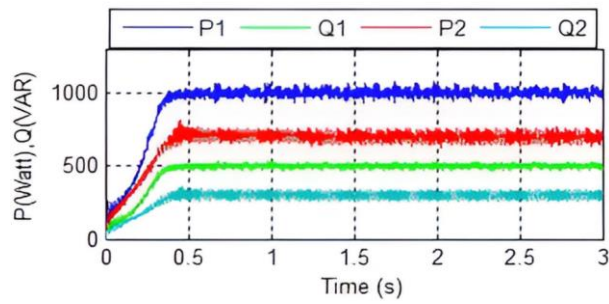
Proportional gain ( $K_p$ )	Integral Gain ( $K_i$ )
0.01	1

##### 4.1 Simulation study

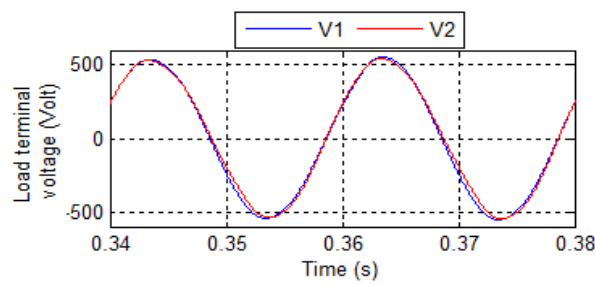
The overall power circuit for conventional and proposed control schemes is realized using MATLAB/SIMULINK software. The input DC voltage is set at 120 V. The standard phase-to-phase load voltage is considered 400 V (r.m.s.) at 50 Hz. The qZSI is operated at two different loading conditions using the suggested control scheme. The active and reactive load power combinations are taken as 1 kW cum 0.5 kVAR and 0.7 kW cum 0.3 kVAR, for two cases. The corresponding powers, voltage, load current ( $I$ ), and shoot-through duty ratio of the simulated system are shown in Figure 3. In Figure 3, the two operating conditions are marked as cases 1 and 2, respectively. This part of the simulation study justifies the successful implementation of the suggested closed loop action to support load variations under the isolated loading condition of qZSI.

The next part of this study verifies the lower value of the voltage stress across any switch using the suggested control scheme and the absence of line-frequency ripple current in the inductor. The DC link voltage is shown in Figure 4(a) using both proposed and traditional MBC-based feedback control schemes under the same loading conditions, i.e., 1 kW and 0.5 kVAR load powers. It is evident from Figure 4(a) that the proposed approach provides a significant reduction in voltage stress in comparison to the MBC-based scheme. Figure 4(b) reveals that the line-frequency ripple current in the inductor is absent in the proposed case, whereas it is present in the MBC case. Then, the simulation study is carried out to demonstrate that the qZSI can support a higher margin of load variation for a limiting value of the boosting factor using the proposed closed loop control scheme than the traditional MBC-based control approach. The load powers are set at 1 kW and 0.5

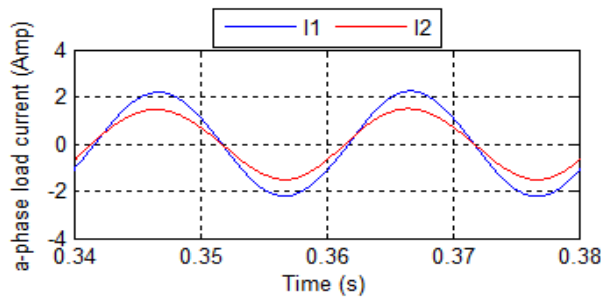
kVAR. The relevant responses are shown and marked in Figure 5. It appears in Figure 5 that the qZSI in the traditional MBC case fails to achieve the target powers, but with the proposed scheme, the qZSI attains these.



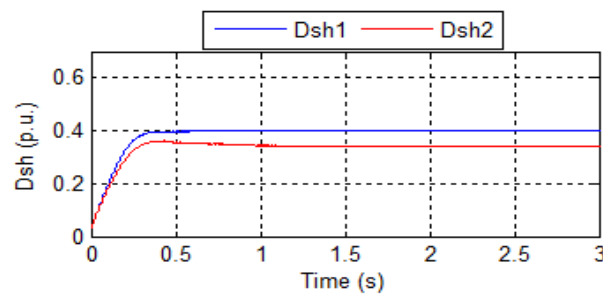
(a) Powers responses



(b) Phase-phase load voltage

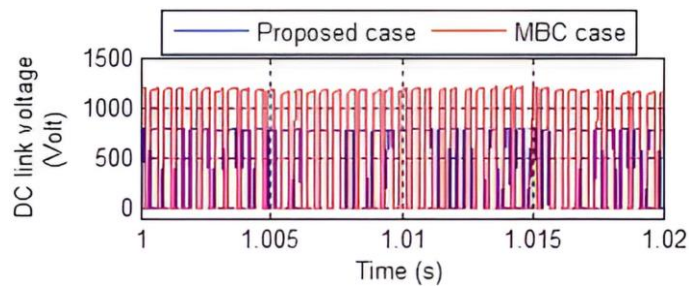


(c) Per-phase load current

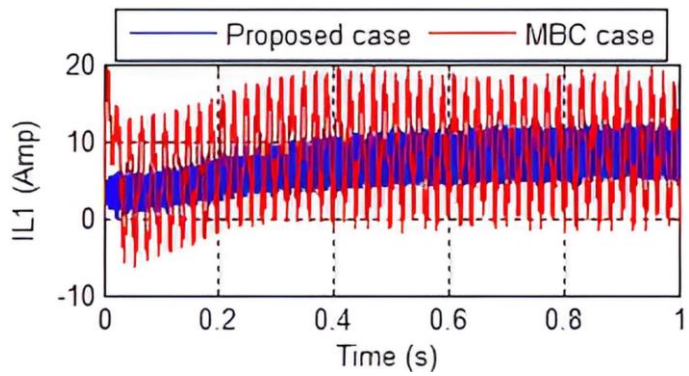


(d) Adaptive shoot-through duty ratios

Figure 3. Various responses under two different loading conditions

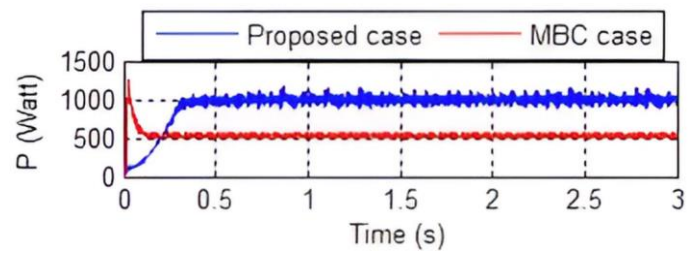


(a) Comparative switch voltage stress under same loading condition

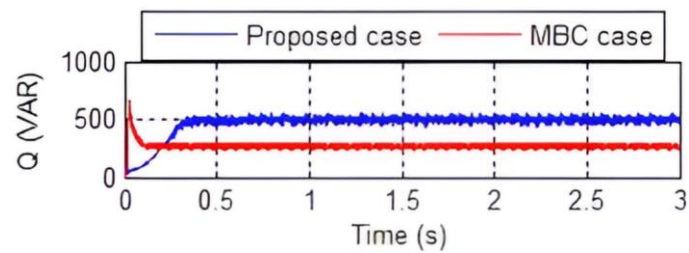


(b) Comparative results showing current through ' $L_1$ '

Figure 4. Comparative performances



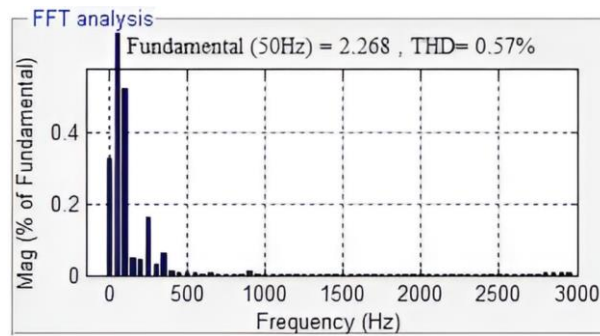
(a) Active power responses



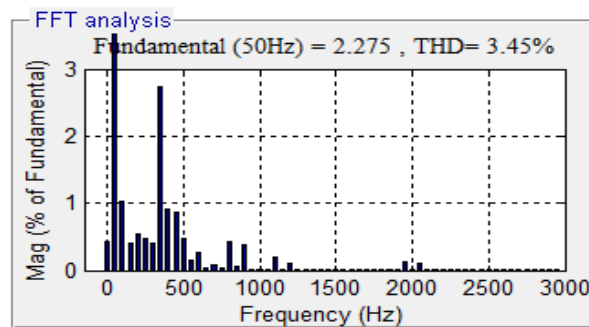
(b) Reactive power responses

Figure 5. Comparative power responses for limiting value of  $B=6.25$

Figure 6 represents the FFT spectra of the load currents under both the proposed and MBC case studies. Figure 6 shows that the THD is lower in the proposed case.



(a) Proposed case



(b) MBC case

Figure 6. FFT spectra of load currents

#### 4.2 Experimental study

The three-phase, 2 kW qZSI is used to perform the hardware experiment. The insulated gate bipolar transistor (IGBT) is used as a power semiconductor switch. The three-phase load box, which has switched resistors and inductors, is used for loading the qZSI. The standard load voltage is like that of the simulation study. The active (P) and reactive (Q) load powers are taken as 1.0 kW and 0.5 kVAR, respectively. The input DC voltage is taken as 120 V. The switching frequency is set at 10 kHz. The real-time controller board dSPACE 1104 is used to generate the control signals using the proposed and MBC control logics developed in MATLAB-SIMULINK software. The Hall-effect voltage sensor LV 25-P is employed to measure the load voltage for the closed loop scheme. The experimental set-up is shown in Figure 7. The hardware results are presented in Figure 8 and Figure 9.

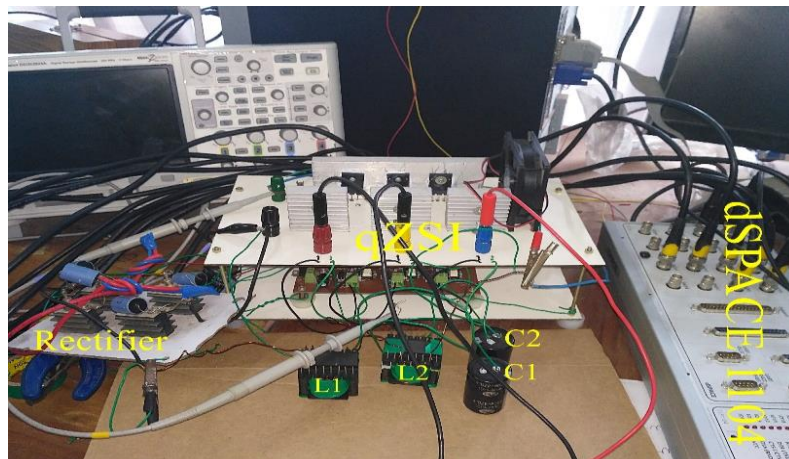
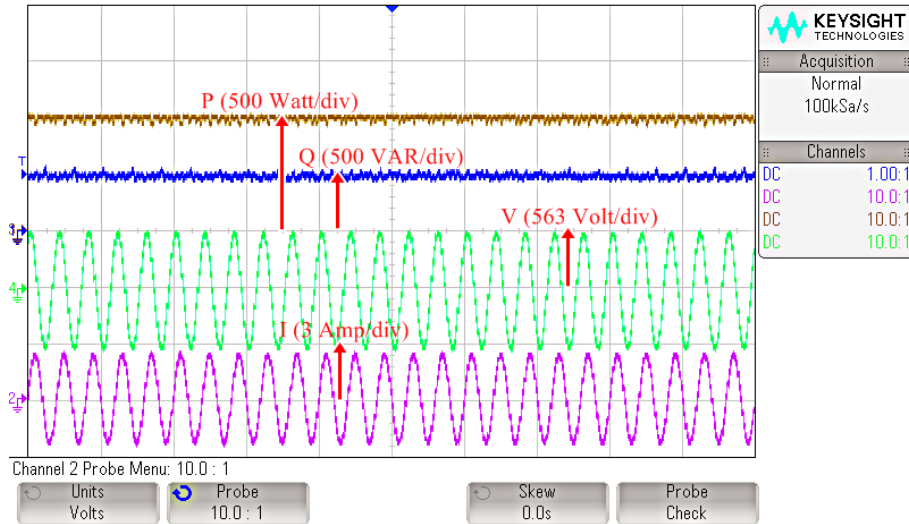
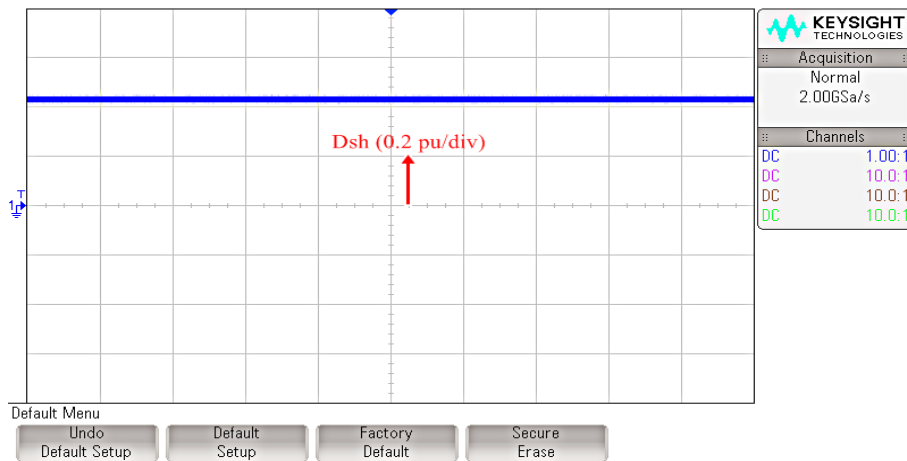


Figure 7. Experimental set up

Figure 8 shows the steady-state load powers, phase-to-phase load voltage, corresponding a-phase load current, and controlled shoot-through duty ratio under the loading conditions mentioned before.

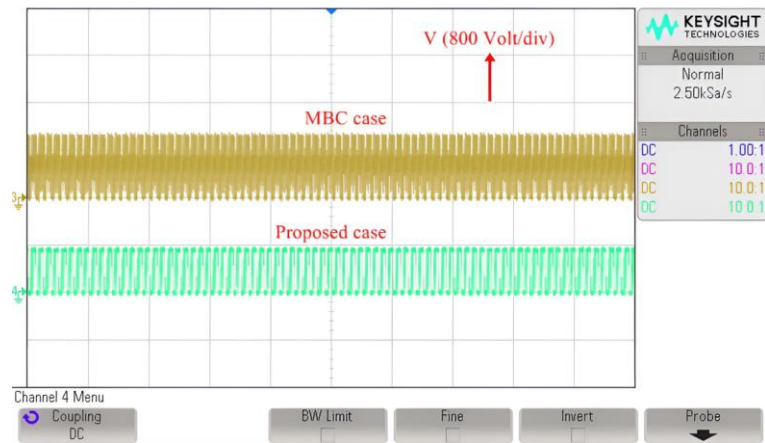


(a) Powers, phase-phase load voltage, and per phase current

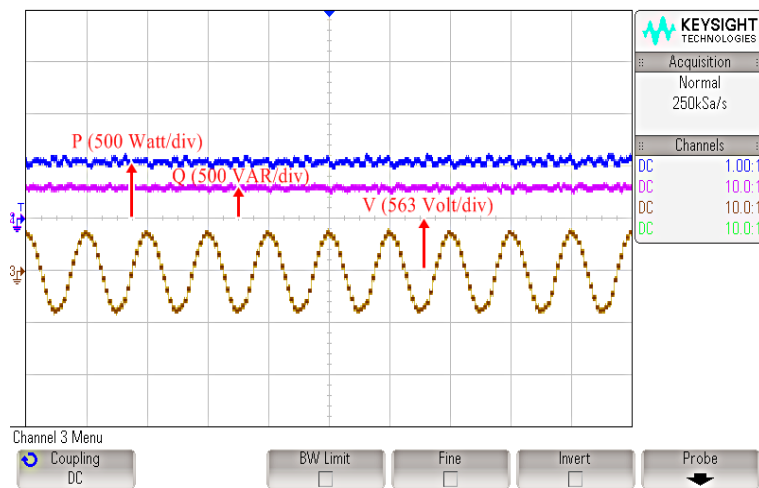


(b) Shoot-through duty ratio

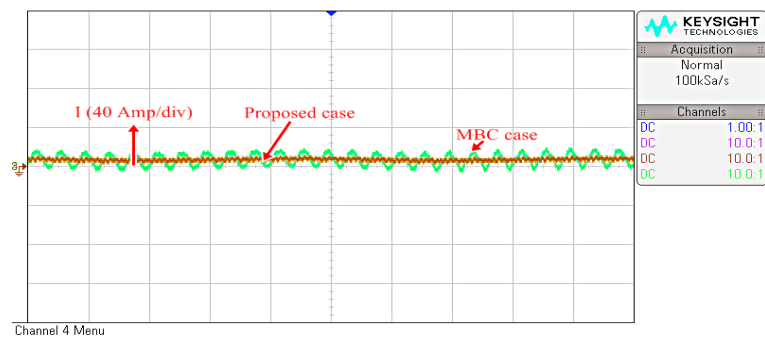
Figure 8. Various results in hardware platform at a particular loading condition



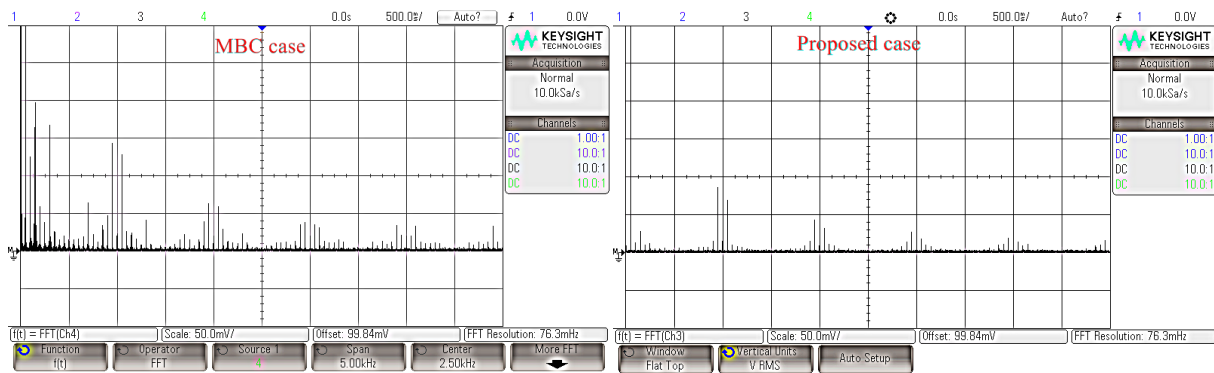
(a) Comparative voltage stress profile in experiment



(b) Powers and voltage responses using MBC technique for limiting value of  $B=6.25$



(c) Comparative results on line frequency ripple current



(d) Comparative FFT spectrums

Figure 9. Various comparative responses for limiting value of  $B=6.25$

It appears from Figure 9(a) that the peak value of the DC link input voltage of the inverter is reduced significantly in the proposed case in comparison with the MBC case for the same loading condition. The load powers and voltage responses shown in Figure 8 are maintained by the proposed logic with a threshold value of boosting factor. The Figure 9(b) shows that the required load powers (1.0 kW and 0.5 kVAR) and voltage (400 V r.m.s) are not maintained by MBC-based technique for the same limiting value of the boosting factor. Figure 9(c) verifies the absence of line-frequency ripple in the inductor current in the proposed case. On the other hand, in Figure 9(c), this low frequency inductor current is present in the MBC-based control approach. Figure 9(d) presents the obtained FFT spectra of the line current for both the proposed and MBC approaches. It is evident from Figure 9(d) that the harmonic contents of the load current are lower in the proposed case in comparison with the MBC-based case study. From the above results of both simulation and experimental work, it can be stated that the proposed closed loop approach shows superior performance over the traditional scheme for improving multiple important practical aspects of qZSI under isolated variable loading conditions. Therefore, the inverter with proposed control logic can be used for supplying AC load powers from DC microgrid and other applications [23, 24]. Table 6 presents comparative performances.

Table 6. Comparisons

Item	Conventional Control [19]		Proposed Control	
	DC-side boost gain (pu)	THD (%)	DC-side boost gain (pu)	THD (%)
Load powers (kW, kVAR)				
1.0, 0.5	6.25	3.4	4.81	1.58
0.8, 0.5	6.25	3.7	4.62	1.69
1.0, 0.6	6.25	3.3	4.96	1.52

## 5 Conclusion

An improved PI controller-based closed loop control methodology with adaptive shoot-through duty ratio adjustment for stand-alone qZSI has been described in this paper. In the proposed logic, the controlled variable is considered a shoot-through duty ratio only for maintaining a constant load voltage profile to meet variable load demands. Here, the logic reduces the voltage stress of power semiconductor switches as well as supporting a higher range of load variation in comparison with that of traditional closed loop schemes. In addition to this, no line-frequency ripple current has been produced in the inductor, and the THD of line current is kept lower by using the proposed closed loop approach. The closed loop control concept, with its improved performances, has been validated successfully on both simulation and experimental platforms. Therefore, it proves the usefulness of the proposed closed loop control scheme for any qZSI-based stand-alone system. The stability of the proposed control scheme will be studied and analysed in future.

## References

- [1] N. Priyadarshi, D. K. Dhaked, I. B. M. Taha, and M. G. Hussien, "Performance Evaluation of Solar-PV-Based Non-Isolated Switched-Inductor and Switched-Capacitor High-Step-Up Cuk Converter," *Electronics*, vol. 11, no. 9, pp. 1381, Apr. 2022.
- [2] Y. Zhang, J. Liu, and C. Zhang, "Comparison of traditional two-stage buck-boost voltage source inverter" in *Twenty-Seventh Annual IEEE Appl. Power Electron. Conf. Expo.*, 5-9 Feb. 2012, pp. 141-148.
- [3] F. Z. Peng, "Z-source inverter," *IEEE Trans. Ind. Appl.*, vol. 39, no. 2, pp. 504-510, Mar./Apr. 2003.
- [4] F. Z. Peng, X. Yuan, X. Fang, and Z. Qian, "Z-source inverter for adjustable speed drives," *IEEE Trans. Power Electron.*, vol. 1, no. 2, pp. 33-35, Jun. 2003.
- [5] F. Z. Peng, A. Joseph, J. Wang, M. Shen, L. Chen, Z. Pan, E. O. Rivera, and Y. Huang, "Z-source inverter for motor drives," *IEEE Trans. Power Electron.*, vol. 20, no. 4, pp. 857-863, Jul. 2005.
- [6] S. Rajakaruna and L. Jayawickrama, "Steady-state analysis and designing impedance network of Z-source inverters," *IEEE Trans. Ind. Electron.*, vol. 57, no. 7, pp. 2483-2491, Jul. 2010.
- [7] J. B. Liu, J. G. Hu, and L. Y. Xu, "Dynamic modeling and analysis of Z-source converter-derivation of ac small signal model and design oriented analysis," *IEEE Trans. Power Electron.*, vol. 22, no. 5, pp. 1786-1796, Sep. 2007.
- [8] H. Rostami, D. A. Khaburi, "Voltage Gain Comparison of Different Control Methods of the Z-Source Inverter" *Elect. and Electron. Engg Conf. (ELECO)*, 5-8 Nov. 2009, pp. I-268-I-272.
- [9] Y. Li, J. Anderson, F. Z. Peng, and D. Liu, "Quasi-Z-source inverter for photovoltaic power generation systems," in *Proc. 24th Annual IEEE APEC*, Feb. 15-19, 2009, pp. 918-924.
- [10] Y. Li, S. Jiang, J. G. Cintron-Rivera, and F. Z. Peng, "Modeling and control of quasi-Z-source inverter for distributed generation applications," *IEEE Trans. Ind. Electron.*, vol. 60, no. 4, pp. 1532-1541, Apr. 2013.
- [11] B. Ge, H. Abu-Rub, F. Z. Peng, Q. Li, A. T. de Almeida, F. J. T. E. Ferreira, D. Sun, and Y. Liu, "An energy stored quasi-Z-source inverter for application to photovoltaic power system," *IEEE Trans. Ind. Electron.*, vol. 60, no. 10, pp. 4468-4481, Oct. 2013.
- [12] L. Yang, D. Qiu D, B. Zhang, G. Zhang, "High-performance quasi-Z-source inverter with low capacitor voltage stress and small inductance," *IET Power Electron.*, vol. 8, no. 6, pp. 1061-1067, Jun. 2015.
- [13] Y. P. Siwakoti, F. Z. Peng, F. Blaabjerg, P. C. Loh, G. E. Town, and S. Yang "Impedance Source Networks for Electric Power Conversion Part II: Review of Control and Modulation Techniques," *IEEE Trans. Power Electron.*, vol. 30, no. 4, pp. 1887-1906, Apr. 2015.
- [14] X. Ding, Z. Qian, S. Yang, B. Cui, and F. Z. Peng, "A direct peak DC-link boost voltage control strategy in Z-source inverter," in *Proc. IEEE Appl. Power Electron. Conf.*, Mar. 2007, pp. 648-653.
- [15] X. Ding, Z. Qian, S. Yang, B. Cui, and F. Z. Peng, "A PID control strategy for DC-link boost voltage in Z-source inverter," in *Proc. IEEE Appl. Power Electron. Conf.*, Mar. 2007, pp. 1145-1148.
- [16] G. Sen and M. E. Elbuluk, "Voltage and current-programmed modes in control of Z-source converter," *IEEE Trans. Ind. Appl.*, vol. 46, no. 2, pp. 680-686, Mar./Apr. 2010.
- [17] P. C. Loh, M. J. Newman, D. N. Zmood, and D. G. Holmes, "A comparative analysis of multiloop voltage regulation strategies for single and three-phase UPS systems," *IEEE Trans. Power Electron.*, vol. 18, no. 5, pp. 1176-1185, Sep. 2003.
- [18] Y. Li and F. Z. Peng, "AC small signal modeling, analysis and control of quasi-Z-source converter," in *Proc. IEEE Power Electron. Motion Control Conf.*, Jun. 2012, pp. 1848-1854.
- [19] C. J. Gajanayake, D. M. Vilathgamuwa, and P. C. Loh, "Development of a comprehensive model and a multi-loop controller for Z-source inverter DG systems," *IEEE Trans. Ind. Electron.*, vol. 54, no. 4, pp. 2352-2359, Aug. 2007.
- [20] F. Z. Peng, M. Shen, and Z. Qian, "Maximum boost control of the Z-source inverter," *IEEE Trans. Power Electron.*, vol. 20, no. 4, pp. 833-838, Jul. 2005.
- [21] M. Shen, J. Wang, A. Joseph, F. Z. Peng, L. M. Tolbert, and D. J. Adams, "Maximum constant boost control of the Z-source inverter," in *Proc. IEEE Annu. Ind. Appl. Conf.*, Oct. 2004, pp. 142-147.

- 
- [22] Y. Liu, B. Ge, H. Abu-Rub, "Theoretical and experimental evaluation of four spacevector modulations applied to quasi-Z-source inverters," *IET Power Electron.*, vol. 6, no. 7, pp. 1257-1269, Aug. 2013.
  - [23] D. K. Dhaked, Y. Gopal, and D. Birla, "Battery Charging Optimization of Solar Energy Based Telecom Sites in India," *Engineering, Technology & Applied Science Research*, vol. 9, no. 6, pp. 5041-5046, Dec. 2019.
  - [24] D. K. Dhaked, and D. Birla, "Modeling and control of a solar-thermal dish-stirling coupled PMDC generator and battery based DC microgrid in the framework of the ENERGY NEXUS" *Energy Nexus, Elsevier*, vol. 5, pp. 100048, Mar. 2022.